ISSN 0023-1584, Kinetics and Catalysis, 2009, Vol. 50, No. 6, pp. 797–815. © Pleiades Publishing, Ltd., 2009.
Original Russian Text © A.S. Ivanova, 2009, published in Kinetika i Kataliz, 2009, Vol. 50, No. 6, pp. 831–849.

Physicochemical and Catalytic Properties of Systems Based on CeO_2

A. S. Ivanova

Boreskov Institute of Catalysis, Siberian Branch, Russian Academy of Sciences, Novosibirsk, 630090 Russia
e-mail: iva@catalysis.ru

Received October 13, 2008

Abstract—The effect of synthesis conditions, the nature of components, and the ratio between the components on the phase composition, the texture, and the redox and catalytic properties of the Ce–Zr–O, Ce–Zr–M_1–O (M_1 = Mn, Ni, Cu, Y, La, Pr, or Nd), *N*/Ce–Zr–O (*N* = Rh, Pd, or Pt), and Pd/Ce–Zr–M_2–O/Al_2O_3 (M_2 = Mg, Ca, Sr, Ba, Y, La, Pr, Nd, or Sm) was considered. A cubic solid solution with the fluorite structure was formed on the introduction of <50 mol % zirconium into CeO_2, and the stability of this solid solution depended on preparation procedure and treatment conditions. The presence of transition or rare earth elements in certain concentrations extended the range of compositions with the retained fluorite structure. The texture of the Ce–Zr–O system mainly depended on treatment temperature. An increase in this temperature resulted in a decrease in the specific surface area of the samples. The total pore volume varied over the range of 0.2–0.3 cm^3/g and depended on the Ce/Zr ratio. The presence of transition or rare earth elements either increased the specific surface area of the system or made it more stable to thermal treatment. The introduction of the isovalent cation Zr^{4+} into CeO_2 increased the number of lattice defects both on the surface and in the bulk to increase the mobility of oxygen and facilitate its diffusion in the $Ce_{1-x}Zr_xO_2$ lattice. The catalytic properties of the Ce–Zr–M_1–O or *N*/Ce–Zr–M_2–O systems were due to the presence of anion vacancies and the easy transitions $Ce^{4+} \rightleftharpoons Ce^{3+}$, $M_1^{2n+} \rightleftharpoons M_1^{n+}$, and $N^{\delta+} \longrightarrow N^0$ in the case of noble metals.

DOI: 10.1134/S0023158409060020

INTRODUCTION

Cerium oxides and cerium-based compounds are used or are going to be used in more than 20 branches of industry. They are employed in the manufacture of refractory materials and ceramic powders, radio ceramics, luminophors, solid electrolytes, supports and catalysts [1]. CeO_2 is most widely used in the utilization of harmful emissions [2, 3]. The applicability of CeO_2 to perform hydrogenation reactions [4, 5], steam reforming [6, 7], CO oxidation [8], hydrocarbon oxidation [9–11], nitrogen oxide reduction with ammonia [12], and hydrogen generation by ethanol reforming [13] has been actively studied. The behavior of CeO_2 in the course of soot removal from the exhaust gases from diesel engines is of considerable interest [14]. Cerium dioxide is also a key component of three-way catalysts (TWCs) [15].

CERIUM OXIDES

Cerium forms the following two compounds with oxygen: Ce_2O_3 and CeO_2 [16]. The oxide Ce_2O_3 has a hexagonal lattice of the La_2O_3 type (space group $P\bar{3}m1$), in which oxygen atoms form closest-packed cubic structure, and cerium atoms are arranged in octahedral voids so that two layers are filled and one layer is empty. The unit cell has the following parameters: a = 3.88 Å and c = 6.06 Å [17] or, according to other data, a = 3.889 Å and c = 6.054 Å [18]. The ionic radius of Ce^{3+} is 1.02 or 1.18 Å according to Belov–Bokii or Goldschmidt, respectively [19]. The heat of formation of Ce_2O_3 is ΔH^0_{298} = 182.1 kJ/mol; its specific density is 6.87 g/cm^3, and melting temperature in an atmosphere of hydrogen is 2433 K. Note that Ce_2O_3 is instable in air. Usually, it is prepared by the reduction of cerium dioxide [16]

$$2CeO_2 + H_2 \longrightarrow Ce_2O_3 + H_2O; \quad \text{(I)}$$

$$2CeO_2 + C \longrightarrow Ce_2O_3 + CO; \quad \text{(II)}$$

$$2CeO_2 + CO \longrightarrow Ce_2O_3 + CO_2. \quad \text{(III)}$$

The stability of the resulting Ce_2O_3 in air depends on the conditions of reactions (I)–(III). For example, Ce_2O_3 prepared in accordance with reaction (I) at 1523–1573 K is spontaneously oxidized in air. However, if the reduction is performed at 2073–2273 K in an atmosphere of purified hydrogen, the resulting oxide becomes stable under ordinary conditions (760 Torr and 298 K). Leonov [16] demonstrated that Ce_2O_3 obtained at 1523–1573 K in accordance with reaction (II) was stable, whereas that obtained via reaction (III) was unstable.

Cerium dioxide has a face-centered cubic lattice of the fluorite (CaF_2) type (space group $Fm3m$). The unit cell parameter a is 5.4110 ± 0.0005 [16] or 5.4113 Å [20]. The ionic radius of Ce^{4+} is 0.88 or 1.02 Å according to Belov–Bokii or Goldschmidt, respectively [19]. The heat of formation of CeO_2 is $\Delta H^0_{298} = 108.9$ kJ/mol; the specific density is 7.3 g/cm^3, and the melting temperature is 2998 K.

A structural peculiarity of fluorite [21] is that the cationic sublattice remains stable even under conditions when the oxygen matrix is dramatically changed. The removal of an atom from the anion packing has no effect on both the face-centered arrangement of the cations and the coordination of the remaining anions. Anion deficiency resulted only in a decrease in the coordination number of individual metal atoms. The total valence of cations should decrease in order to retain the total neutrality of the compound. Thus, fluorite can be described by the general formula MO_{2-x} depending on the number of anion vacancies.

According to published data [22], the fluorite structure is stable only at the ratio between cationic and anionic radii $r_c/r_a > 0.732$, whereas this ratio in CeO_2 is much smaller. Because the stability of the test structure suggests the occurrence of a larger cation, it is believed that an amount of Ce^{3+} cations, whose ionic radius according to Belov–Bokii is 1.02 Å [19], occurs in the structure along with Ce^{4+}. In turn, the presence of Ce^{3+} results in the appearance of anionic vacancies (CeO_{2-x}).

The results of XPS studies suggest the occurrence of various valence states in the structure of CeO_2. According to these results, a partial electron transfer from the occupied $2p$ orbital of the O atom to the unoccupied O^{2-} $4f_0$ (Ce^{4+}) orbital was observed [23, 24]. However, Wuilloud et al. [25] disputed this statement. Theoretical calculations [26, 27] showed that a co-valence occurs in the structure of CeO_2. Nevertheless, for simplicity, it is believed [28, 29] that CeO_2 is formally a purely ionic compound, which consists of Ce^{4+} and O^{2-} ions, even on the surface. Nonstoichiometric oxides CeO_{2-x} ($0 < x < 0.5$) are readily formed on heating CeO_2 in a vacuum or on reducing it with hydrogen or CO at moderate temperatures [30]. Oxygen vacancies are the predominant defects responsible for the nonstoichiometry of CeO_2 [31], which manifests itself in its behavior as an n-type semiconductor [32]. According to calculations, the concentration of oxygen vacancies on the surface is greater than that in the bulk [33]. Upon the partial removal of oxygen, O^- vacancies appear in the structure of CeO_2; the other electrons can be localized in the conduction band or distributed over several $Ce^{\delta+}$ cations to surround them so that an O^- vacancy is produced, or they are localized on Ce^{4+} to form Ce^{3+} [29]. The complete discrete localization of excess electrons of individual Ce^{3+} ions was most correctly described by Conesa [29].

Thus, the structure of CeO_2 can accumulate the major portion of oxygen vacancies with no structural changes. This corresponds to the transformation $CeO_2 \rightleftharpoons CeO_{2-x} + x/2O_2$. This property of CeO_2 is responsible for its so-called oxygen storage capacity (OSC), which is related to the occurrence of the redox pair Ce^{4+}/Ce^{3+}. The key role of CeO_2 as the constituent of TWCs is explained by the fact that, because of its redox properties, it readily removes CO and hydrocarbons from automobile exhaust gases in a deficiency of oxygen (reactions (IV)–(VI)) and adsorbs and retains oxygen from O_2, NO, and water (reactions (VII)–(IX)) in the subsequent cycles [34]. This makes it possible to successfully utilize the main pollutants (CO, HC, and NO) under typical operation conditions of TWCs.

$$CeO_2 + xCO \longrightarrow CeO_{2-x} + xCO_2; \quad \text{(IV)}$$

$$CeO_2 + HC \longrightarrow CeO_{2-x} + (H_2O, CO_2, CO, H_2); \quad \text{(V)}$$

$$CeO_2 + xH_2 \longrightarrow CeO_{2-x} + xH_2O; \quad \text{(VI)}$$

$$CeO_{2-x} + xNO \longrightarrow CeO_2 + 0.5xN_2; \quad \text{(VII)}$$

$$CeO_{2-x} + xH_2O \longrightarrow CeO_2 + xH_2; \quad \text{(VIII)}$$

$$CeO_{2-x} + 0.5xO_2 \longrightarrow CeO_2. \quad \text{(IX)}$$

However, at high temperatures, CeO_2 is unstable; this primarily manifests itself as changes in its texture characteristics. Upon thermal treatment (1000–1100 K), the specific surface area (S_{BET}) of CeO_2 usually decreased to a few square meters per gram depending on preparation conditions and calcination regime [35, 36]. It is of importance that CeO_2 is a more expensive support than Al_2O_3 and SiO_2. Therefore, CeO_2 is mainly used in combination with other oxides.

The nature and concentration of the introduced component are crucial factors in the modification of CeO_2. According to published data [37], compositions with various defects are formed upon the introduction of cations with higher or lower valences into CeO_2:

$$2MO + Ce_{Ce} \longrightarrow 2M_{Ce} + CeO_2 + 2V_0,$$

$$2M_2O_3 + 3Ce_{Ce} \longrightarrow 4M_{Ce} + 3CeO_2 + 2V_0,$$

where M is a divalent or trivalent cation, Ce_{Ce} is the cerium cation in a cerium position in the lattice of CeO_2, M_{Ce} is the introduced metal cation in a cerium position in the lattice of CeO_2, and V_0 is a vacancy. The introduction of a trivalent cation increases the mobility of oxygen to a greater extent than the introduction of a bivalent cation. CeO_2 can readily enter into reactions with titanium and zirconium dioxides, as well as with rare earth elements and transition metals, to form corresponding solid solutions. The Ce–Zr–O system has been studied in most detail [38–59].

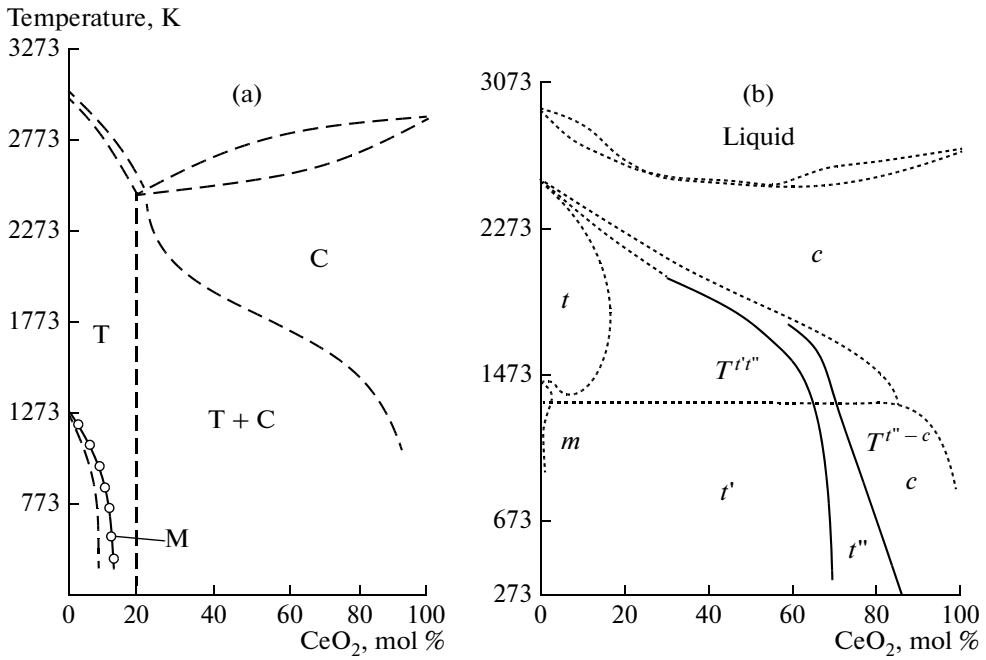

Fig. 1. Phase diagrams of the CeO_2–ZrO_2 system: data taken from (a) [39] and (b) [40].

Ce–Zr–O SYSTEM

Phase Composition

A comparison between the ionic radii of cerium and zirconium (r_{Ce}^{4+} = 0.88 Å; r_{Zr}^{4+} = 0.82 Å) and the structural isomorphism of CeO_2 and ZrO_2 allow one to hypothesize that the introduction of zirconium into the structure of cerium dioxide will be accompanied by the formation of solid solutions. Indeed, it follows from a phase diagram [39] that three types of solid solutions (monoclinic, tetragonal, and cubic) are formed in the above system and stoichiometric compounds are absent from this system (Fig. 1a). According to a refined phase diagram [40] (Fig. 1b), a single-phase region with monoclinic (*m*) symmetry occurs below 1273 K, where the mole fraction of CeO_2 is lower than 10%. Only a cubic (*c*) phase, which was also mentioned previously [41, 42], is formed at a CeO_2 content higher than 80%. The medium region of the CeO_2–ZrO_2 phase diagram, where the greatest number of stable and metastable phases with tetragonal symmetry was observed, is most complicated and ambiguous [43–45]. According to published data [40] based on X-ray and Raman characteristics, three phases, *t, t'*, and *t"*, can be recognized here. The stable *t* form results from the occurrence of diffusion processes; the formation of the metastable *t'* form is a consequence of diffusion changes, whereas the *t"* form occupies an intermediate position between *t'* and cubic forms. It is not tetragonal, and an oxygen shift with respect to the ideal fluorite structure occurs in it. The *t"* form is often referred to as cubic because, according to a diffraction pattern, it is indexed in the cubic structure with spatial symmetry *Fm3m* [46]. According to published data [40], the region of $Ce_{1-x}Zr_xO_2$ compositions in which this form occurs is broad ($0.1–0.2 < x < 0.30–0.35$). According to Vlaic et al. [47], it can be formed at a CeO_2 content of 50–60 mol %. Thus, depending on the CeO_2 content, five modifications (one monoclinic, three tetragonal, and one cubic) can occur in the Ce–Zr–O system.

The occurrence of metastable phases in the medium part of the phase diagram essentially depends on the method of synthesis of mixed oxides and kinetic factors: the lability or inertness of the system. This was supported by Turko et al. [48], who found that samples with close chemical compositions but precipitated at different temperatures (293 and 343 K) exhibited different phase compositions. As can be seen in Fig. 2 and Table 1, the sample precipitated at room temperature was single-phase, and it can be described in terms of both cubic and tetragonal structures (the tetragonal distortion is small, a/c = 0.99). The above data are consistent with the results of published studies [47, 49], in which it was found that a tetragonal phase is formed in the region of Ce/Zr ≈ 1, and this phase cannot be distinguished from a cubic phase in terms of XRD analysis. The Ce/Zr ratio, which was found from unit cell parameters (Table 1), was similar to the chemical composition of the tetragonal structure.

An increase in the precipitation temperature to 343 K resulted in the formation of two phases: one of them was a cubic phase with a high cerium dioxide content ($Ce_{1-x}Zr_xO_{2-\delta}$, where x = 0.20–0.27), and

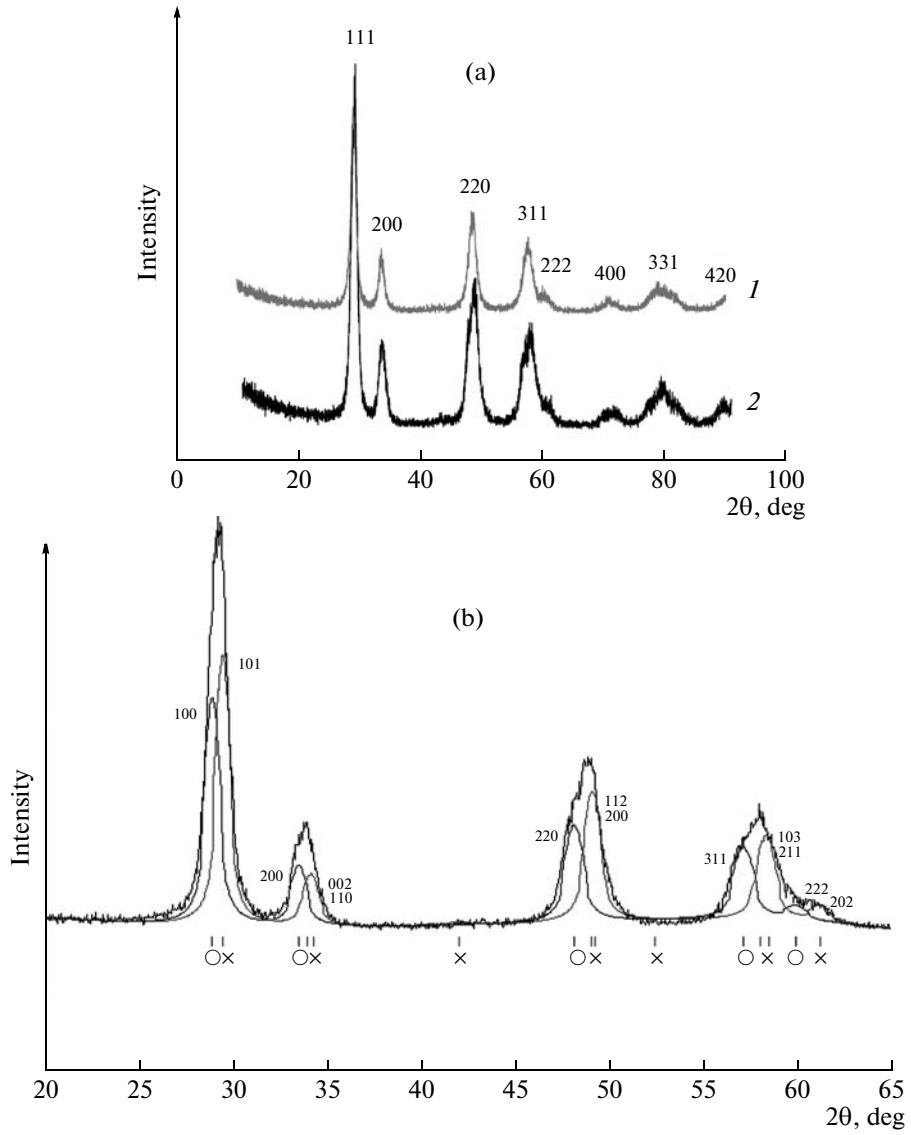

Fig. 2. (a) Diffraction patterns of cerium–zirconium samples with Ce/Zr ratios of (*1*) 1.08 and (*2*) 1.17 precipitated at (*1*) 293 and (*2*) 343 K and calcined at 1173 K. (b) Comparison of the experimental diffraction pattern of a cerium–zirconium sample with the ratio Ce/Zr = 1.08 calcined at 1173 K with the calculated diffraction patterns of (○) cubic $Ce_{0.78}Zr_{0.22}O_2$ and (×) tetragonal $Ce_{0.37}Zr_{0.66}O_2$ [48].

the second phase can be interpreted in two manners, as in the case of a single-phase sample. In Table 1, it can be seen that the R_p factor, which characterizes the discrepancy between the experimental diffraction patterns and diffraction patterns theoretically calculated based on well-known structures taken from the ICDS structural database with consideration for diffraction line profiles, was lower for this sample, and a better agreement between the resulting Ce/Zr ratio and the chemical composition suggested the formation of a tetragonal structure.

Different chemical compositions of samples precipitated at different temperatures can be due to different rates of hydrolysis of the starting nitrate salts. As a result of this, for example, the concentrations of nitrates in the resulting systems were different. Previously, it was found [50–52] that the occurrence of anionic groups in the structure of ZrO_2 or CeO_2 facilitated the stabilization of their fluorite-type cubic structures.

The samples prepared by a ceramic method (the thermal treatment of cerium and zirconium dioxides at 1873 K for 1 h) and containing from 10 to 50 mol % CeO_2 consisted of a mixture of phases: tetragonal + monoclinic or tetragonal + cubic. The samples containing more than 50 mol % CeO_2 were single-phase; only a cubic phase was present in them [53]. With the use of a sol–gel method or the coprecipitation of components, the solid solutions of a cubic structure were formed after treatment at lower temperatures.

Table 1. Phase composition of $Ce_{1-x}Zr_xO_2$ samples precipitated at various temperatures [48]

Precipitation temperature, K	Composition	Phase composition at 1173 K	R_p^*	a/c	Refined phase composition
293	$Ce_{0.52}Zr_{0.48}O_2$	100% cubic	16.83	–	$Ce_{0.66}Zr_{0.34}$
		100% tetr.	16.35	0.99	$Ce_{0.49}Zr_{0.51}$
343	$Ce_{0.54}Zr_{0.46}O_2$	15% cubic	16.64	–	$Ce_{0.85}Zr_{0.15}$
		85% cubic			$Ce_{0.56}Zr_{0.44}$
		32.7% cubic	10.40	0.99	$Ce_{0.78}Zr_{0.22}$
		67.3% tetr.			$Ce_{0.37}Zr_{0.63}$

* R_p factor characterizes the discrepancy between experimental and calculated data.

Typical diffraction patterns of a solid solution containing from 67 to 100 mol % CeO_2 and calcined at 973 K (Fig. 3a) are characterized by the presence of broad reflections [49]. This suggests a low degree of crystallinity of the particles; however, these particles have a cubic structure based on CeO_2. The diffraction pattern of a solid solution containing 16 mol % CeO_2 exhibited reflections corresponding to a tetragonal phase. The samples calcined at 1173 K (Fig. 3b) were better crystallized, and the intensity of reflections in their spectra was higher. The unit cell parameter a, which was calculated from the corresponding indices of a cubic lattice, depended on the composition of the solid solution (Fig. 4). The value of a linearly decreased as the ZrO_2 content was increased from 0 to 33 mol % ZrO_2; that is, Vegard's rule was obeyed, according to which the introduction of a cation with a smaller radius ($r_{Zr^{4+}} = 0.82$ Å, whereas $r_{Ce^{4+}} = 0.88$ Å) causes the above change in this parameter. This suggests that solid solutions up to $Ce_{0.67}Zr_{0.33}O_2$ are crystallized in cubic or pseudocubic structures, as noted by Vlaic et al. [47]. At the same time, because the diffraction signals of the $Ce_{0.67}Zr_{0.33}O_2$ sample calcined at 1173 K were somewhat asymmetric, it is believed that this composition can consist of a mixture of phases. Indeed, the samples containing 47 mol % CeO_2 contained a mixture of tetragonal and cubic phases; this is consistent with published data [53]. After hydrothermal treatment at 1273 K, the solid solutions remained cubic up to a CeO_2 concentration of 75 mol % (Fig. 5). The (111) reflection remained asymmetric at a CeO_2 concentration of 67 mol %, although reflections due

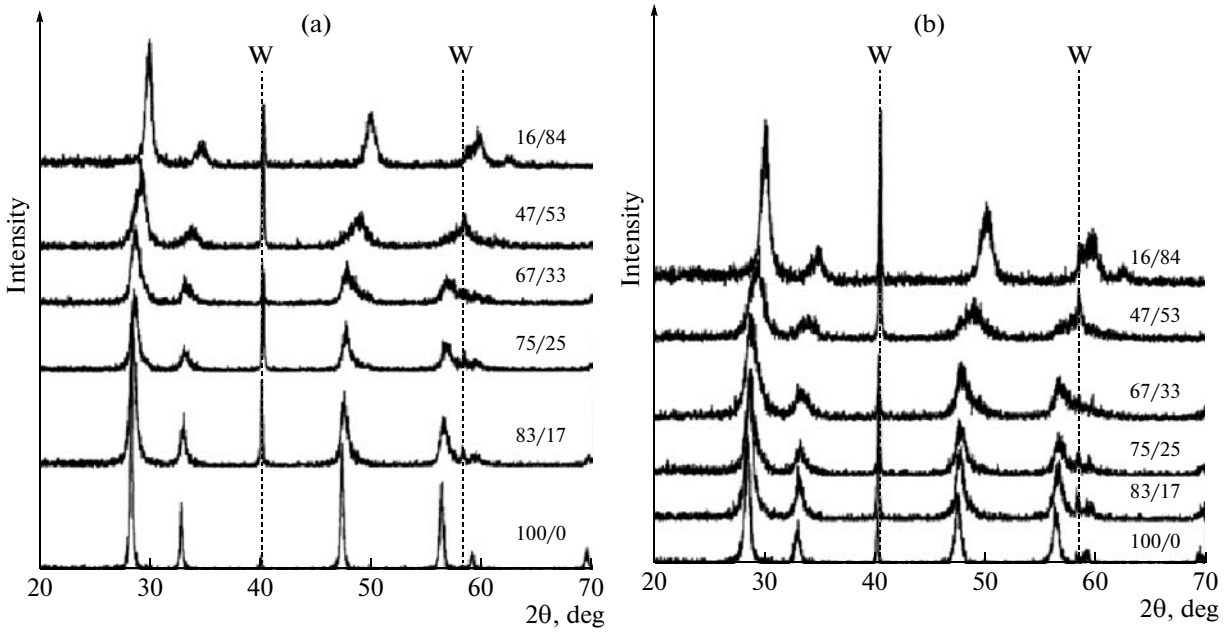

Fig. 3. Diffraction patterns of Ce–Zr–O solid solutions calcined at (a) 973 and (b) 1173 K [49]. The CeO_2/ZrO_2 ratios are specified in the spectra. Tungsten was added as an internal standard.

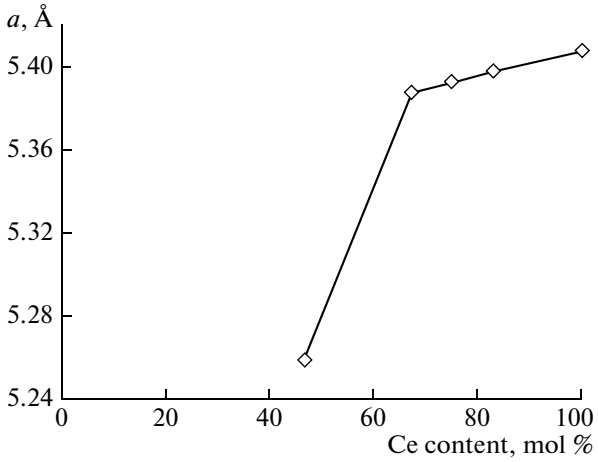

Fig. 4. Dependence of the unit cell parameter a on the cerium content of solid solutions calcined at 1173 K [49].

to a tetragonal phase were not observed in this case. Undoubtedly, the solid solution containing 47 mol % CeO_2 was a mixture of cubic and tetragonal phases, whereas it was purely tetragonal at a CeO_2 concentration of 16 mol %. The results obtained by Hartridge and Bhattacharya [54] provided an additional support to the fact that only a cubic solid solution was formed in the region of $Ce_{1-x}Zr_xO_{2-\delta}$ compositions with $x \leq 0.3$ over a temperature range from 373 to 1273 K; the crystallite size in this solid solution changed from 3.5 to 5.5 nm.

Table 2 shows the effects of the synthesis procedure, the nature and ratio between the initial components, and the treatment temperature on the phase composition of the Ce–Zr–O system. As can be seen,

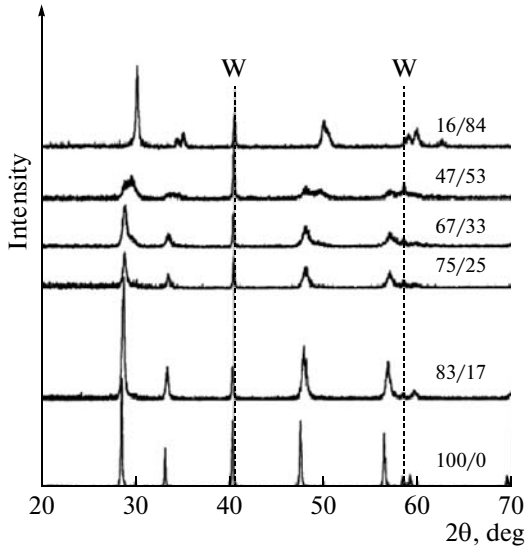

Fig. 5. Diffraction patterns of Ce–Zr–O solid solutions aged at 1273 K [49]. The CeO_2/ZrO_2 ratios are specified in the spectra.

the resulting solid solution had a fluorite-type cubic structure regardless of the above parameters at CeO_2 concentrations of ≥80 mol %, and this structure remained stable up to 1673 K.

Texture Characteristics

Texture formation in the Ce–Zr–O system occurs simultaneously with changes in the phase composition. The specific surface area of cerium–zirconium samples depends on preparation conditions, CeO_2 content, temperature, and atmosphere in which thermal treatment is performed (Table 3) [49, 55, 58, 62]. Composition and treatment temperature play a decisive role in surface formation. Upon the introduction of zirconium into CeO_2, in the majority of cases, an increase in the S_{BET} of binary samples was observed. If the treatment temperature was no higher than 823 K, S_{BET} was 100–120 m^2/g (Table 3) regardless of the ratio between the components. An increase in the treatment temperature caused a decrease in S_{BET} in any synthetic procedure [63]. In particular, the specific surface area of samples calcined at 973 K was as low as 50–70 m^2/g.

After treatment under hydrothermal conditions at 1273 K for 24 h, S_{BET} decreased most significantly [49]: it decreased to 3–8 m^2/g in the case of binary samples. In addition to calcination temperature, treatment time had a considerable effect on the specific surface area [64]. The greatest decrease in S_{BET} occurred in the first hours of calcination during which it decreased from 40–50 to 10–15 m^2/g. A further increase in the calcination time up to 16 h had almost no effect on S_{BET}.

The formation of the pore structure of Ce–Zr–O compositions has received little attention. Note that, as applied to these systems, the following regularity characteristic of oxide systems was retained: more macroporous compositions are also more thermally stable. As can be seen in Fig. 6, both unimodal and bimodal pore-size distributions can be observed in the samples of the same composition. The samples of the

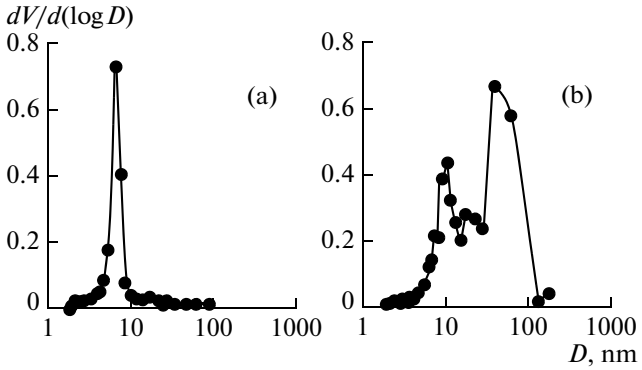

Fig. 6. (a) Unimodal and (b) bimodal pore-size distribution in $Ce_{0.2}Zr_{0.8}O_2$ [65].

Table 2. Effect of synthesis conditions and procedure and calcination temperature on the phase composition of the Ce–Zr–O system

Method	Initial components	Treatment temperature, K	Composition $Ce_{1-x}Zr_xO_2$	Structure*	References
Sol–gel	$Zr(OC_3H_7)_4 + Ce(NO_3)_3$	873	$0 < x < 0.25$	C	[55]
			$x = 0.25$	C	
			$0.25 < x \le 0.5$	$C + T_0$	
			$x = 0.84$	T	
	$Zr(O–Bu)_4 + Ce(acac)_4$	773	$x = 0.50$	C + T	[56, 57]
Precipitation	$ZrO(NO_3)_2 + Ce(NO_3)_3$ or	873	$0 < x \le 0.5$	$C + T_0$	[55]
	$ZrOCl_2 + Ce(NO_3)_3$		$x = 0.84$	T	
	$ZrO(NO_3)_2 + Ce(NO_3)_3$	973	$0 < x \le 0.11$	C	[58]
			$0.11 < x \le 0.50$	$C + C_z$	
			$0.5 < x \le 0.66$	$C + C_z$	
			$0.66 < x \le 0.90$	C_z	
	$Zr(NO_3)_4 + Ce(NO_3)_3$	1173	$x \le 0.20$	C	[59]
			$0.20 \le x \le 0.50$	$C + T_0$	
			$0.85 \le x \le 0.99$	T	
Mixing	$CeO_2 + ZrO_2$	1673	$x \le 0.2$	C	[40, 60, 61]
			$0.20 < x \le 0.80$	T	
			$x > 0.80$	M	

* C, cubic; C_z, cubic based on ZrO_2; T, tetragonal; T_0, tetragonal ZrO_2; and M, monoclinic ZrO_2.

Table 3. Effect of calcination temperature on the specific surface area of CeO_2–ZrO_2 samples

CeO_2 content, mol %	S_{BET} (m^2/g) after calcination at temperature, K								
	823 [61]	873 [54]			673 [57]	973 [57]	973 [48]	1173 [48]	1273* [48]
		from $Zr(OC_3H_7)_4$	from $ZrO(NO_3)_2$	from $ZrOCl_2$	from $ZrO(NO_3)_2 + Ce(NO_3)_3$		from $ZrO(NO_3)_2 + Ce(NO_3)_3$		
100	100	–	47	47	40	25	49	14	1
90–89.5	–	75	46	40	120	50	–	–	–
80–83	111	–	–	–	–	–	58	27	3
75	–	63	57	53	–	–	61	29	5
67–68	100	–	–	–	–	–	70	26	8
60	–	71	73	65	–	–	–	–	–
47–50	106	56	46	44	130	60	62	19	3
33.3	–	–	–	–	140	60	–	–	–
15–16	95	46	74	49	–	–	84	43	1
10	–	–	–	–	150	90	–	–	–
0	–	21	87	36	180	32	57	31	8

* Hydrothermal aging for 24 h in an atmosphere of 5 vol % O_2, 10 vol % H_2O, and 85 vol % N_2.

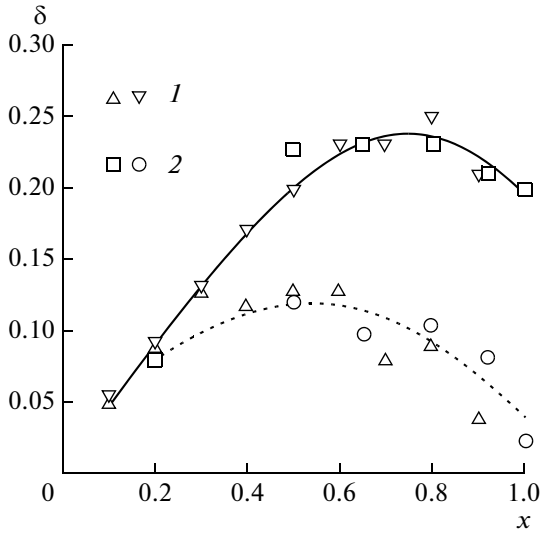

Fig. 7. Degree of reduction of $Ce_xZr_{1-x}O_2$ samples after treatment with a mixture of 5% H_2 with 95% Ar at low (700–900 K, dashed line) and high (1300 K, solid line) temperatures under TPR conditions: (*1*) samples with low S_{BET} and (*2*) samples with high S_{BET} [72].

latter type, which were characterized by a larger average pore diameter, exhibited a higher thermal stability [65]:

Calcination temperature, K	S_{BET} of a unimodal sample, m^2/g	S_{BET} of a bimodal sample, m^2/g
973	65	76
1273	9	20
1373	–	9

The character of changes in the texture characteristics of the samples is of importance in performing reduction cycles [62]: on going from fresh to reduced samples, the isotherms of adsorption changed from type IV to type II. In all cases, porosity decreased after a reductive treatment. The specific surface area decreased in the course of consecutive reduction cycles; however, the degree of this decrease depended on the ratio between the components in the Ce–Zr–O system. After performing consecutive reduction cycles, the texture characteristics of compositions with the ratios $CeO_2/ZrO_2 = 80 : 20$ and $50 : 50$ were considerably impaired, whereas these changes were insignificant at the ratio $CeO_2/ZrO_2 = 15 : 85$.

Redox Properties

The capability to reduction and OSC are very important characteristics of $Ce_{1-x}Zr_xO_{2-\delta}$ systems [53, 62, 66–68]. There are two peaks in the spectrum of the temperature-programmed reduction with hydrogen (H_2 TPR) of fresh CeO_2; one of them corresponds to surface reduction (~773 K), whereas the other corresponds to bulk reduction (~1073 K) [67, 69, 70]. After reductive aging at 1323 K, the signs of low-temperature reduction, which corresponded to about 20% surface, were retained.

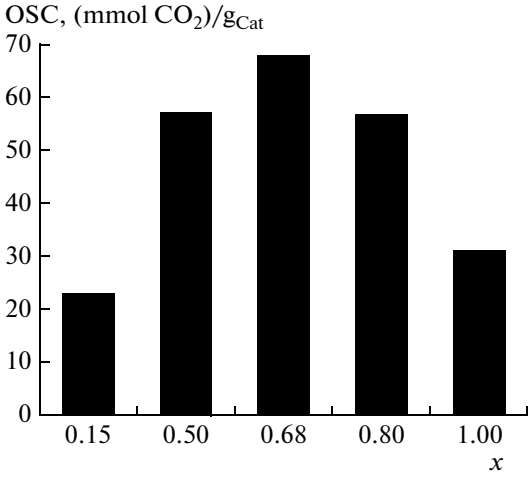

Fig. 8. OSCs of various cerium–zirconium oxides measured at 673 K after the introduction of the first pulse of O_2 [73].

The reduction pattern of a $Ce_{1-x}Zr_xO_{2-\delta}$ solid solution was different: in this case, the low-temperature peak remained unchanged after high-temperature aging, although S_{BET} considerably decreased. A peak at ~950 K appeared in the H_2 TPR spectrum upon the reduction of the $Ce_{0.6}Zr_{0.4}O_2$ solid solution, which was prepared by mixing the corresponding components followed by thermal treatment at 1873 K for 1 h [71]. The total H_2 uptake was 8.2 ml/g and corresponded to the final empirical formula $Ce_{0.6}Zr_{0.4}O_{1.94}$. The coefficient δ in the equation

$$Ce_{1-x}Zr_xO_2 + \delta H_2 = Ce_{1-x}Zr_xO_{2-\delta} + \delta H_2O + \delta V_0 \quad (X)$$

depends on the ratio between components in the solid solution and is almost independent of the surface area (Fig. 7) [72]. A higher degree of reduction resulted in an increase in the intensity of oxygen exchange in solid solutions, as compared with a pure oxide [53]. The total degree of reduction characterized the relative concentration of oxygen thermodynamically accessible at a given temperature.

The specific activity of the Ce–Zr–O composition can be better described by the amount of oxygen absorbed and released by the system in a pulse mode (the consecutive treatment of a sample with oxidizing and reducing mixtures) under real conditions, for example, in the operation of an automobile engine. The results indicate that solid solutions with an intermediate composition can accumulate, store, and release O_2 (OSC) to the greatest extent. As an example, Fig. 8 shows the behavior of Ce–Zr–O solid solutions upon the dosed supply of dynamic pulses of oxygen for the oxidation of CO [73]. The $Ce_{0.5}Zr_{0.5}O_2$

composition is considered an optimum. The reason can be that a balance between the number of reduced centers (Ce atoms) and structural characteristics occurred in this composition. Moreover, it was found [74] that OSC increased with x in the series of $Ce_{1-x}Zr_xO_{2-\delta}$ samples. In fact, the OSC of the $Ce_{0.63}Zr_{0.37}O_2$ sample was higher than the corresponding value for CeO_2 by a factor of about 4. As a rule, an optimum value of OSC was observed in the range of $0.2 \le x \le 0.4$ [74]. A comparison (Fig. 9) showed that the value of OSC at 673 K was proportional to the number of surface oxygen sites. $Ce_{0.63}Zr_{0.37}O_2$ exhibited a maximum number of surface superoxide sites. Thus, we can conclude that sites of the O_2^- type can participate in oxygen transfer and storage. Descorme et al. [75] used IR spectroscopy to study the following three different superoxide sites on the surfaces of CeO_2 and $Ce_{0.63}Zr_{0.37}O_2$: $^{16}O_2^-$, $^{16}O^{18}O^-$, and $^{18}O_2^-$. Theoretical calculations and the results of previous experiments [76, 77] suggest that the states $^{16}O^{18}O^-$ and $^{18}O_2^-$ can be responsible for absorption bands at 1094 and 1062 cm^{-1}, respectively. Surface superoxide sites can be formed as a result of the interaction between molecular oxygen and the reduced Ce^{3+} site. Interactions of this type will result in the reoxidation of Ce^{3+} to Ce^{4+} followed by the formation of O_2^- sites.

Li et al. [76, 77] observed the formation of peroxide sites (O_2^{2-}) on a prereduced surface. They believed that this could be a consequence of interactions between molecular oxygen and two neighboring Ce^{3+} sites. In fact, superoxides can be considered as virtual intermediates in the full cycle of $Ce_{1-x}Zr_xO_{2-\delta}$ reoxidation, in which surface electrons were intensely transferred to the oxygen molecule [75]:

$$O_{2\,gas} \longrightarrow O_{2\,ads} \longrightarrow O_{2ads}^-(\text{superoxide})$$
$$\longrightarrow O_{2ads}^{2-}(\text{peroxide}) \longrightarrow 2O_{ads}^- \longrightarrow 2O_{lattice}^{2-}.$$

Ce–Zr–M–O SYSTEMS

Ce–Zr–M–O Systems with Transition Metals

It is well known that CeO_2 reacts with the transition metal oxides MnO_x, NiO, and CuO to form solid solutions [78–84]. Cerium dioxide forms a solid solution with the fluorite structure with cations with smaller ionic radii (Cu^{2+}, Mn^{3+}, and Mn^{4+}) in a limited region of compositions.

The phase composition of CeO_2–MnO_2 prepared by precipitation and calcined at 650°C depended on the ratio between the components [79–82]: at $Mn/(Ce + Mn) \le 0.5$, a cubic solid solution with the fluorite structure was formed, whose particle size of increased with treatment time, whereas an additional phase of Mn_2O_3 appeared at $Mn/(Ce + Mn) > 0.75$. At the same time, the ratio between the components affected only slightly the texture characteristics of the samples [80, 81]: as the fraction of manganese was increased from 20 to 50%, the value of S_{BET} increased from 48 to 74 m^2/g, and the pore volume and the average pore diameter remained within the ranges of 0.11–0.14 cm^3/g and 64–98 Å, respectively.

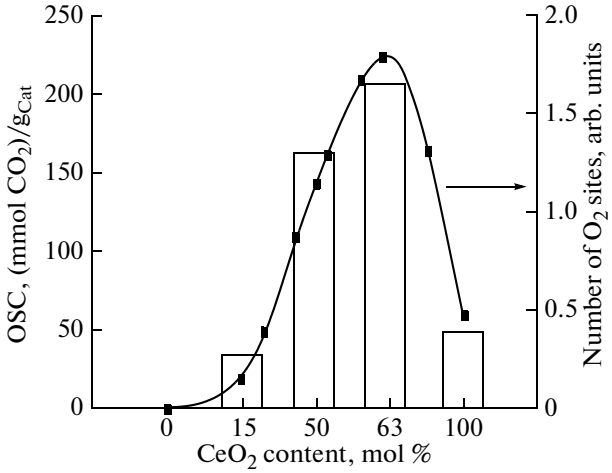

Fig. 9. Correlation between OSC at 673 K and the concentration of superoxides formed after oxygen adsorption on the series of preoxidized $Ce_xZr_{1-x}O_2$ oxides at room temperature [74]. The concentration of superoxides was determined from an absorption band at 1126 cm^{-1} in the IR spectrum.

Lamonier et al. [83] studied the series of CeM_xO_y (M = Ni or Cu) oxides prepared by precipitation and calcined in air at 573 and 1073 K. The introduction of small amounts of Ni or Cu facilitated an increase in S_{BET}. Depending on the nickel content, the oxides $CeNi_xO_y$ can be subdivided into two groups [83, 84]: at $x \le 0.5$, solid solutions were formed with Ni^{2+} ions inserted into the lattice of CeO_2, whereas compositions in which NiO was crystallized along with a solid solution were formed at $x > 0.5$. The Cu/Ce atomic ratio on the surface of $CeCu_xO_y$ oxides depends on the depth of analysis. The experimental results can be explained by the formation of CuO and/or small particle size of CuO and the insertion of the Cu^{2+} ion into the cerium dioxide matrix. At a low copper content ($x < 0.5$), CuO was not formed; this oxide appeared along with $CeCu_xO_y$ at a higher Cu/Ce ratio.

The introduction of Ni^{2+} or Cu^{2+} into cerium dioxide decreased the temperature of reduction, as compared with pure CeO_2. Because, according to published data [84], the reduction of a solid solution resulted in the coexistence of M^0, M^+, M^{2+}, Ce^{3+}, and Ce^{4+}, it is believed that the process passed through the following steps:

(1) M^{2+}, which occurred in the structure of a solid solution, was reduced to M^+ or M^0;

(2) as a result of water release, new anionic vacancies in the lattice of CeO_2 were generated;

Table 4. Effect of rare earth element additives on the stability of the Ce–Zr–O system [91]

Composition, wt %	S_{BET} (m^2/g) after calcination at temperature, K			
	1173	1273	1373	1473
$70CeO_2$–$30ZrO_2$	45	20	5	<1
$58CeO_2$–$42ZrO_2$	45	19	4	<1
$60CeO_2$–$30ZrO_2$–$3La_2O_3$–$7Pr_6O_{11}$	56	40	23	6
$20CeO_2$–$75ZrO_2$–$2.5La_2O_3$–$2.5Nd_2O_3$	65	44	10	<1

(3) the simultaneous reoxidation of M^0 or M^+ was accompanied by the reduction $Ce^{4+} \longrightarrow Ce^{3+}$;

(4) anionic vacancies were occupied by H_2 with the possible formation of hydride complexes.

The reduction of M^{2+} or M^+ in a solid solution occurred at lower temperatures, as compared with the reduction of Ce^{4+}, to facilitate the formation of a greater number of anionic vacancies [85]. Takeguchi et al. [86] studied the reducing properties of the NiO/CeO_2–ZrO_2 system and found that, upon the addition of a small amount (0.6 wt %) of NiO, the peak of H_2 absorption in the TPR spectrum of the $NiO/Ce_{0.25}Zr_{0.75}O_2$ sample shifted toward lower temperatures (from 653 to 543 K). As the fraction of NiO was increased to 12.4 wt %, a further increase in the reduction temperature to 453 K was observed. Takeguchi et al. [86] believed that NiO promoted the reduction of the sample. The low-temperature reduction of the support also occurred in the simultaneous occurrence of Ni and platinum group metals; usually, this was explained by the effect of hydrogen spillover [87, 88].

Ce–Zr–M–O Systems with Rare Earth Elements

It was demonstrated above that, as a rule, the $Ce_{1-x}Zr_xO_{2-\delta}$ systems with x from 0.2 to 0.4 exhibited the highest oxygen capacity. However, because CeO_2 is comparatively expensive, the recent trend has been toward decreasing its concentration in the test compositions on condition that the fluorite structure is retained. From a phase diagram, it follows that the formation of a solid solution with a tetragonal structure became possible as the fraction of cerium dioxide was decreased; consequently, the fluorite structure should be additionally stabilized. It is well known [89] that alkaline earth or rare earth element ions can serve as stabilizers. Of rare earth elements, Y. La, and Pr are best suited for the preparation of solid solutions with cerium–zirconium oxides [67, 90].

The introduction of the trivalent cations Y^{3+} or La^{3+} into the lattice of a Ce–Zr–O solid solution makes it possible to retain its cubic structure at a low CeO_2 content (30 mol %). All of the resulting samples exhibited relatively high S_{BET} (70–75 m^2/g) and consisted of particles of size 5–7 nm; that is, modification had almost no effect on the above characteristics.

The introduction of lanthanum cations decreased the consumption of hydrogen in the course of TPR, whereas the introduction of yttrium increased it. At the same time, the temperature at which a maximum rate of reduction was reached (T_{max}) did not depend on the presence or absence of a trivalent cation.

The Ce–Zr–Pr–O composition containing 70 wt % CeO_2, 30 wt % ZrO_2, and 5 wt % Pr_7O_{11} was more stable than the above system with no Pr [67]. In this composition, unlike Ce–Zr–O, phase segregation did not occur after aging in air at 1323 K, and S_{BET} remained unchanged or even somewhat increased after reduction and aging. The simultaneous introduction of lanthanum and neodymium or lanthanum and praseodymium into the Ce–Zr–O system even greater increased its thermal stability (Table 4) [91]. However, an increase in thermal stability was not accompanied by an increase in the OSC of the Ce–Zr–Pr–O composition, as compared with the Ce–Zr–O oxide. Thus, the introduction of ~5 wt % praseodymium into the Ce–Zr–O system stabilized the fluorite structure more efficiently than the introduction of yttrium or lanthanum, but it had no effect on the character of reduction and, consequently, on the value of OSC.

The simultaneous yttrium and lanthanum promotion of Ce–Zr–O compositions with the Ce/Zr ratios from 0.26 to 0.62 facilitated the formation of a single-phase solid solution with the fluorite structure at 873 K, which was retained after heating at 1423 K [48]. On the one hand, the stabilization effect of the fluorite structure upon the simultaneous introduction of Y^{3+} and La^{3+} cations was due to their ionic radii, which are greater than the ionic radii of Ce^{4+} and Zr^{4+} and approach the ionic radius of Ce^{3+}. On the other hand, the above cations form solid solutions with the fluorite structure with cerium and zirconium dioxides [90, 92].

The specific surface area of (Ce, Zr, Y, La)O_{2-x} solid solutions also mainly depends on treatment temperature: S_{BET} = 50–80 and 0.6–0.8 m^2/g at 873 and 1423 K, respectively. The temperature-programmed reduction of samples calcined at 873 K with hydrogen occurred in two steps; this may be explained by the initial occurrence of surface reduction and then bulk

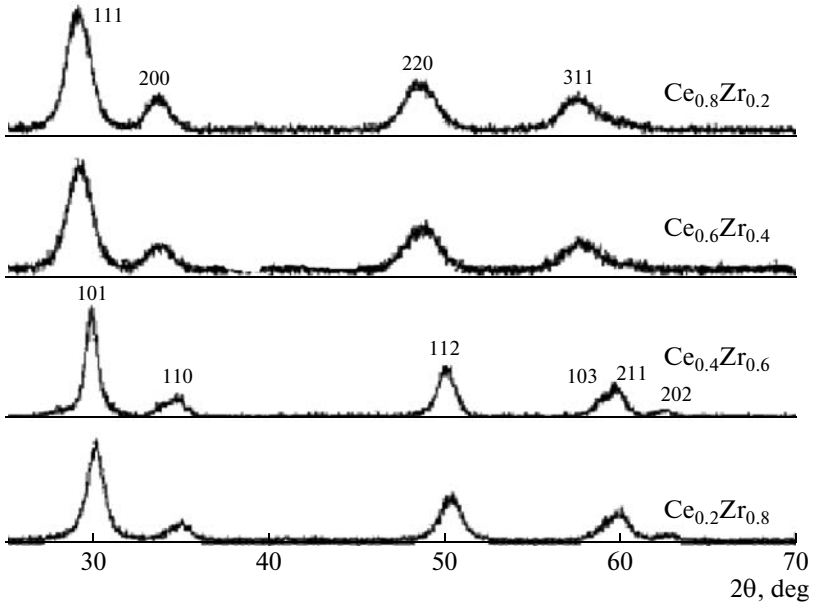

Fig. 10. Diffraction patterns of cerium–zirconium samples from series M [101].

reduction. The samples with the ratios Ce/Zr = 0.26 and 0.40 calcined at 1423 K were reduced in a single step at 980 and 859 K, respectively; in this case, the lower the Ce/Zr ratio, the higher the degree of reduction.

The additional introduction of transition metal cations (Mn, Fe, and Co) into this complex composition did not change the structure of the samples if they were precipitated at room temperature [93]. In the samples of Ce–Zr–Y–La–Fe(Co)–O precipitated at 343 K and calcined at 1423 K, two solid solutions with cubic and tetragonal structures were formed. The presence of transition metal cations in Ce–Zr–Y–La–M–O samples facilitated a decrease in the reduction temperature and the appearance of a low-temperature peak in the H_2 TPR spectrum in the range of 423–573 K. Cobalt is the most efficient additive. An analogous effect was also observed in the samples containing platinum group metals.

N/Ce–Zr–O Systems with Rh, Pd, and Pt

According to published data [94–98], the $Ce_{1-x}Zr_xO_2$ solid solution is a good support for platinum group metals, which serve as catalysts for the reactions of complete methane oxidation, methane and ethanol reforming, etc. The reduction of cerium–zirconium compositions containing these metals occurred at lower temperatures. That is, the presence of platinum group metals, as well as transition metals, facilitated the low-temperature reduction of the bulk of solid solution because of the spillover of hydrogen, which was transferred from the metal additive to the Ce-containing component [99, 100]. The degree of this effect depends on both the Ce–Zr–O preparation method and the supporting and concentration of a platinum group metal.

Ho et al. [101] compared the properties of $Pd/Ce_xZr_{1-x}O_2$ catalysts with a Pd content of 0.8 wt %, which were different in support synthesis procedures. The cerium–zirconium supports were prepared by two procedures: (1) template synthesis from a mixture of $Zr(OC_3H_7)_4$ + $(NH_4)_2Ce(NO_3)_6$ in the presence of cetyltrimethylammonium bromide (CTAB) (series M) and (2) coprecipitation of the solutions of $CeCl_3$ and $ZrCl_4$ (series C). The prepared samples were dried and calcined at 973 K. Palladium was supported by impregnating the support followed by thermal treat-

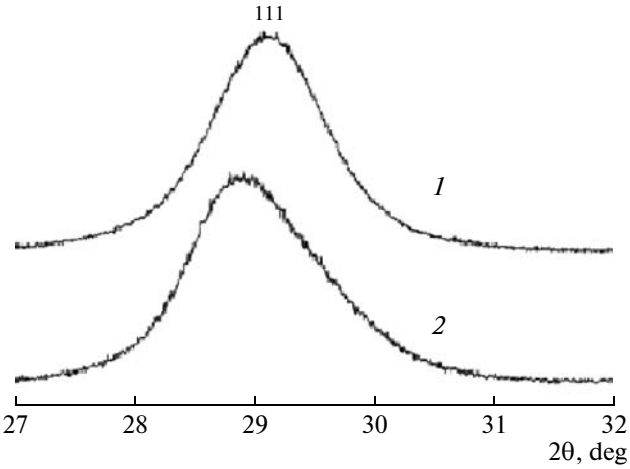

Fig. 11. Diffraction patterns of $Pd/Ce_{0.6}Zr_{0.4}O_2$ samples from series M and C.

Table 5. Effect of treatment temperature and preparation procedure on the texture characteristics of $Pd/Ce_{0.6}Zr_{0.4}O_2$ samples [101]

Sample	Treatment temperature, K	S_{BET}, m^2/g	V, cm^3/g	Pore diameter, nm
$Pd/Ce_{0.6}Zr_{0.4}O_2$ (ser M)	773	131	0.14	4.2
	873	103	0.18	7.0
	973	69	0.16	10.0
	1073	57	0.14	10.1
$Pd/Ce_{0.6}Zr_{0.4}O_2$ (ser C)	973	21	0.05	10.8

Table 6. Structure, texture, and catalytic properties of $Pd/Ce_{0.6}Zr_{0.4}O_2$ samples prepared by various methods [101]

Preparation method	M	C
Rate of CO oxidation at 60°C, mol s^{-1} g^{-1}	5.3×10^{-7}	1.9×10^{-7}
T_{50}, K	338	370
T_{90}, K	348	393
S_{BET} at 973 K, m^2/g	69	21
Crystal structure	cubic	cubic + tetrahedral

ment. According to XRD data, the supporting of palladium onto the Ce–Zr–O composition from series M did not cause structural changes in the samples (Fig. 10); the structure depended on the CeO_2 content. An increase in the fraction of CeO_2 from 20 to 80% was accompanied by a structural transformation from tetragonal to cubic; the PdO phase was absent. However, the structures of $Pd/Ce_{0.6}Zr_{0.4}O_2$ samples from series M and C were different (Fig. 11): (111) peak asymmetry in the spectrum of the sample from series C suggests the presence of a tetragonal solid solution based on ZrO_2, whereas this peak in the spectrum of the sample from series M had a symmetric shape, which suggests the formation of a cubic solid solution based on CeO_2. The texture characteristics of samples prepared by both of the procedures were different (Table 5). In samples from series M, S_{BET} decreased with treatment temperature; the average pore diameter increased, and the pore volume nonmonotonically changed. The specific surface area and pore volume of samples from series M and C calcined at 973 K differed by a factor of about 3, whereas the average pore diameters were similar. Consequently, the introduction of CTAB at the support preparation stage allowed one to prepared more dispersed and thermally stable Pd-containing catalysts, which had an increased activity (Table 6). The temperatures at which 50 and 90% conversions were reached (T_{50} and T_{90}, respectively) were 338 and 348 K, respectively, for this sample. In this case, the rate of CO oxidation on this catalyst was higher by a factor of 2.8 than that on the sample whose support was prepared by coprecipitation.

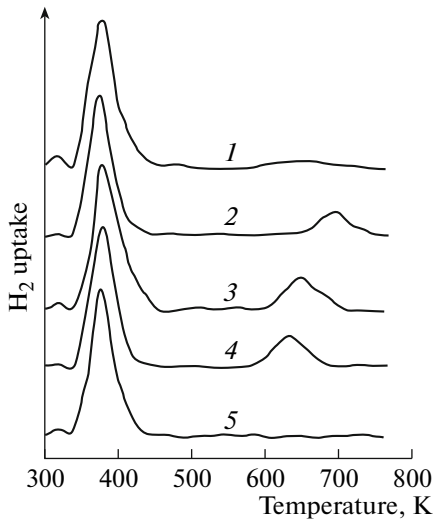

Fig. 12. H_2 TPR curves of samples prepared by the precipitation of palladium (17% Pd) [102]: (*1*) Pd/CeO_2, (*2*) $Pd/Ce_{0.9}Zr_{0.1}O_2$, (*3*) $Pd/Ce_{0.8}Zr_{0.2}O_2$, (*4*) $Pd/Ce_{0.5}Zr_{0.5}O_2$, and (*5*) Pd/ZrO_2.

An increase in the Pd content to 17 wt % and a change in the supporting procedure from precipitation (prec) to impregnation (impr) resulted in changes in the phase composition and the redox properties of the $Pd/Ce_{1-x}Zr_xO_2$ catalyst [102]. According to XRD data, the $Pd/Ce_{1-x}Zr_xO_2$(prec) and $Pd/Ce_{1-x}Zr_xO_2$(impr) with a Pd content of 17 wt % dried at 373 K for 24 K and calcined at 723 K for 3 h had the fluorite structure [102], whose unit cell parameter is $a = 5.412$ Å. The exception is the $Ce_{0.8}Zr_{0.2}O_2$ catalyst, in which $a =$

5.364 Å. Note that the structures of ZrO_2 and PdO are different from cubic. The PdO phase was detected only in the $Pd/Ce_{0.8}Zr_{0.2}O_2$(impr) sample rather than in Pd/CeO_2(prec) and $Pd/Ce_{0.8}Zr_{0.2}O_2$(prec). The procedure of supporting Pd strongly affected its average particle size [102]: it was 5–6 nm in the $Pd/Ce_{0.8}Zr_{0.2}O_2$(prec) sample; this size is smaller than that in $Pd/Ce_{0.8}Zr_{0.2}O_2$(impr) and Pd/CeO_2(prec).

After the reduction of the Pd/CeO_2(prec), $Pd/Ce_{0.8}Zr_{0.2}O_2$(prec), and $Pd/Ce_{0.8}Zr_{0.2}O_2$(impr) at 673 K for 1 h, the XRD spectrum exhibited a peak due to Pd^0. The unit cell parameters of $Pd/Ce_{0.8}Zr_{0.2}O_2$ (prec) and $Pd/Ce_{0.8}Zr_{0.2}O_2$ (impr) became somewhat larger, and those of Pd/CeO_2 (prec) remained almost unchanged.

The H_2 TPR curves of $Pd/Ce_{1-x}Zr_xO_2$ (impr) (x = 0, 0.1, 0.2, 0.5) show a peak in the temperature range from 373 to 423 K, which is assignable to Pd^{2+} reduction (Fig. 12) [102]. Moreover, upon the reduction of samples with different Ce/Zr ratios prepared by palladium precipitation, peaks in the region of 600–700 K appeared; these peaks suggest the partial reduction of the support $Ce_{1-x}Zr_xO_2$ ($Ce^{4+} \longrightarrow Ce^{3+}$). The H_2 TPR curves of the Pd/CeO_2(prec) and Pd/ZrO_2(prec) samples exhibited no peaks due to the reduction of $Ce(Zr)O_2$ at temperatures higher than 873 K (Fig. 12). Thus, as the Zr^{4+} content was increased, the Ce^{4+} reduction peak shifted toward lower temperatures. The introduction of the Zr^{4+} cation into the CeO_2 lattice facilitated the formation of defects both on the surface and in the bulk, and these defects increased the mobility and diffusion of oxygen in the lattice; in turn, this facilitated the reduction of Ce^{4+} in the $Ce_{0.8}Zr_{0.2}O_2$ solid solution [10]. According to published data [103, 104], the joint action of Zr^{4+} and Pd^{2+} facilitated the reduction of Ce^{4+} in the $Pd/Ce_{0.8}Zr_{0.2}O_2$(prec) sample at 600–700 K.

The character of reduction of $N/Ce_{0.68}Zr_{0.32}O_2$ samples, where N = Rh, Pd, or Pt, also depends on the nature of the metal [105]. The predominance of low-temperature reduction was typical of all of these samples. In the case of $Pd/Ce_{0.68}Zr_{0.32}O_2$ and $Rh/Ce_{0.68}Zr_{0.32}O_2$, this was related to the previous reduction of a supported platinum group metal oxide, which made possible the spillover of hydrogen to facilitate the reduction of the support. In the $Pt/Ce_{0.68}Zr_{0.32}O_2$ sample, the reduction of the support occurred at a higher temperature because surface platinum oxide is more difficult to reduce [106].

Let us consider the effect of the nature of the platinum group metal on an important characteristic of cerium–zirconium systems such as OSC. Hickey et al. [105] studied the $N/Ce_{0.68}Zr_{0.32}O_2$ and CeO_2 catalysts and found that the mechanism of formation of their ability to absorb, store, and release oxygen also depends on the nature of the reducing agent (H_2 or CO). With the use of H_2 as a reducing agent, considerable values of dynamic OSC with the formation of H_2O were reached at room temperature. This was due to the ability of hydrogen to spillover in the presence of a metal that activates H_2. In this respect, Rh, Pd, and Pt were the most efficient. The higher thermal stability of $Ce_{1-x}Zr_xO_2$ systems, as compared with CeO_2, indicated that the value of OSC remained significant even after considerable reductive aging.

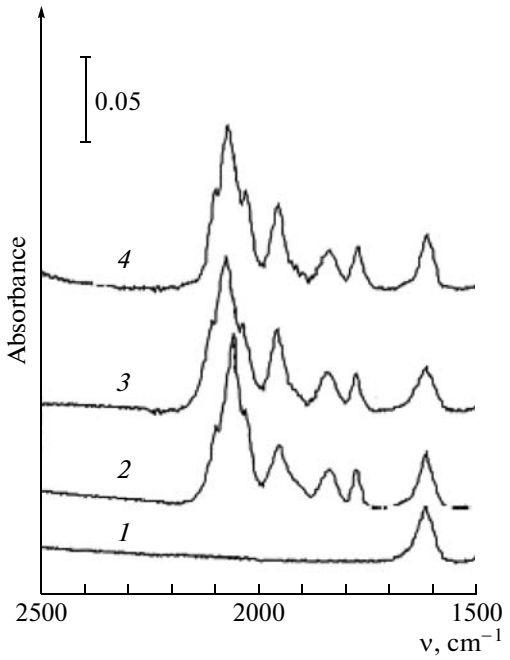

Fig. 13. IR spectra of CO adsorbed on (*1*) $Ce_{0.8}Zr_{0.2}O_2$, (*2*) 17% Pd/CeO_2(prec), (*3*) 17% $Pd/Ce_{0.8}Zr_{0.2}O_2$(prec), and (*4*) 17% $Pd/Ce_{0.5}Zr_{0.5}O_2$(prec) after pumping at room temperature for 30 min [102].

If CO was the reducing agent, the dynamic OSC exhibited a complex behavior because the adsorption and desorption of CO occurred in the course of surface reduction. On the fresh (oxidized) $Pt/Ce_{0.68}Zr_{0.32}O_2$ catalyst with a high S_{BET}, considerable values of OSC were reached only at temperatures higher than 473 K. If the catalyst was prereduced at 500 K, a noticeable OSC effect with the participation of CO was observed even at 373 K. At the same time, the OSC effect was not detected on samples with low S_{BET} below 673 K. Unlike platinum and palladium, rhodium promoted the reduction of the support with carbon monoxide.

The IR spectra of CO adsorbed on $Ce_{0.8}Zr_{0.2}O_2$, Pd/CeO_2(prec), $Pd/Ce_{0.8}Zr_{0.2}O_2$(prec), and $Pd/Ce_{0.5}Zr_{0.5}O_2$(prec) were somewhat different (Fig. 13). Upon the adsorption of CO on $Ce_{0.8}Zr_{0.2}O_2$, an absorption band at 1617 cm^{-1} appeared, which corresponds to the formation of surface carbonates [107]. The introduction of Pd changed the character of CO adsorption: the spectrum of Pd/CeO_2(prec) exhibited absorption bands at 2072, 2099, 2030, 1955, 1840, and 1777 cm^{-1}. The first five bands belong to the vibrations

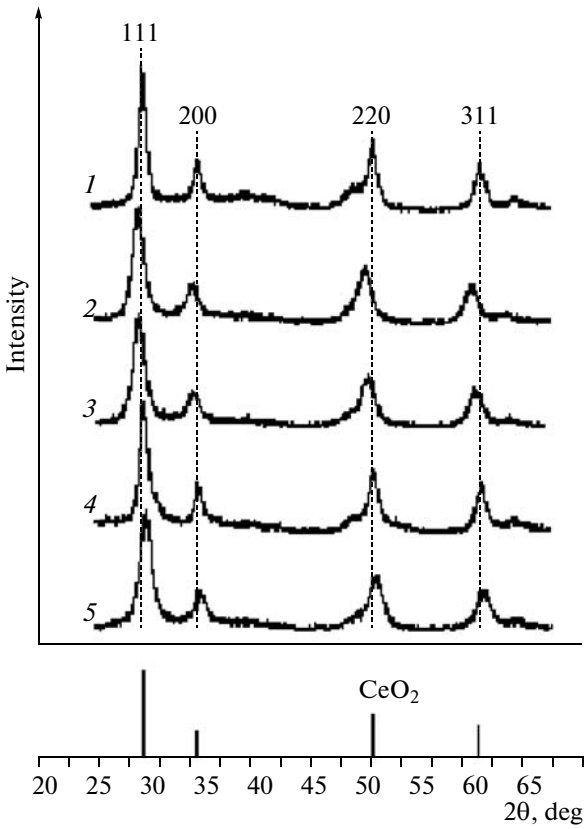

Fig. 14. Diffraction patterns of the following samples [111]: (*1*) Pd/Al–Ce–O, (*2*) Pd/Al–Ce–La–O, (*3*) Pd/Al–Ce–Ca–O, (*4*) Pd/Al–Ce–Zr–O, and (*5*) Pd/Al–Ce–Mg–O.

of linear monocarbonyl, symmetric and asymmetric dicarbonyls, and bridging CO, which was formed as a result of a transformation of the linear form of this oxide [108], whereas the absorption band at 1777 cm^{-1} can be attributed to the CO molecule bound to surface palladium through an oxygen atom [109]. Upon the adsorption of CO on $Pd/Ce_{0.8}Zr_{0.2}O_2$(prec) and $Pd/Ce_{0.5}Zr_{0.5}O_2$(prec), analogous absorption bands appeared; however, the band due to linear CO complexes shifted to 2088 and 2084 cm^{-1}, respectively. Thus, the character of CO adsorption on the surfaces of the test samples depended on the Ce/Zr ratio.

$Pd/Ce–Zr–M–O/Al_2O_3$ Systems with Alkaline Earth and Rare Earth Elements

The cerium–zirconium composition in combination with aluminum oxide is of considerable practical importance. A typical TWC consists of a honeycomb cordierite support and a supported layer several tens of micrometers in thickness (washcoat), which contains Al_2O_3 as a support for noble metals, mainly Pt(Pd) and Rh in a ratio of 5 : 1 and a Ce–Zr–O composition as an oxygen buffer material [110]. Therefore, attention has been focused on studying the formation of these complex systems.

Xiao et al. [111] prepared 2% Pd catalysts by the deposition of palladium onto a support precalcined at 873 K; the support contained 70 wt % Al_2O_3 + 30 wt % (CeO_2–MO_n), where M = Mg, Zr, Ca, or La. In turn, the support was synthesized by the precipitation of cerium nitrates and a corresponding component (at the ratio Ce/M = 4) onto suspended γ-Al_2O_3 followed by washing, drying, and calcination. Reflections due to PdO or MO_n were absent from the diffraction patterns of the samples (Fig. 14). The general view of the spectra suggests the formation of a solid solution with the fluorite structure, whose unit cell parameters increased with the ionic radius of the introduced M: Pd/Al–Ce–Mg–O < Pd/Al–Ce–Zr–O < Pd/Al–Ce–O < Pd/Al–Ce–Ca–O < Pd/Al–Ce–La–O. Moreover, although the fraction of Al_2O_3 in the given composition was higher than the fraction of a Ce-containing component, the Al_2O_3 peak intensity was insignificant. As was found using XRD analysis, the particle size of the solid solution in the Pd/Al–Ce–O sample was 12 nm, and it decreased to 7.6 nm upon the introduction of La. The palladium particle size, which was measured using the chemisorption of CO, also decreased from 5.1 to 2.9 nm upon the introduction of promoting additives in the order Pd/Al_2O_3 < Pd/Al–Ce–O < Pd/Al–Ce–Mg–O < Pd/Al–Ce–Zr–O ≈ Pd/Al–Ce–Ca–O < Pd/Al–Ce–La–O. Thus, the introduction of promoting additives into a Ce-containing component increased the degree of dispersion and, consequently, the activity of Pd [111]. Indeed, the activity of catalysts in the reaction of CH_4 oxidation changed in the same order as the degree of dispersion of Pd:

System	Pd/Al_2O_3	Pd/Al–Ce	Pd/Al–Ce–Mg	Pd/Al–Ce–Zr	Pd/Al–Ce–Ca	Pd/Al–Ce–La
T_{50}, °C:	349	346	345	344	340	318

Similar results were obtained in studies of the more complicated 0.5% $Pd/Ce–Zr–M/Al_2O_3$ systems (M = Mg, Ca, Sr, Ba, Y, La, Pr, Nd, and Sm) [112, 113], in which the concentration of a cerium–zirconium component (Ce/Zr = 1 : 4) was 18 wt %, which is lower than that in [111] by a factor of ~1.7. Moreover, the concentration of M was also lower. The catalysts were prepared by the impregnation of the support calcined at 1173 K with a solution of H_2PdCl_4 followed by drying and calcination at 773 K. The support

Table 7. Specific surface areas of supports and Pd/Ce–Zr–M–O/Al_2O_3 catalysts [112, 113]

Support calcined at 1173 K	S_{BET}, m^2/g	Catalyst calcined at 1373 K	S_{BET}, m^2/g
Al_2O_3	98	Pd/Al_2O_3	25
Ce–Zr–O/Al_2O_3	106	Pd/Ce–Zr–O/Al_2O_3	49
Ce–Zr–Mg–O/Al_2O_3	111	Pd/Ce–Zr–Mg–O/Al_2O_3	52
Ce–Zr–Ca–O/Al_2O_3	112	Pd/Ce–Zr–Ca–O/Al_2O_3	54
Ce–Zr–Sr–O/Al_2O_3	116	Pd/Ce–Zr–Sr–O/Al_2O_3	60
Ce–Zr–Ba–O/Al_2O_3	118	Pd/Ce–Zr–Ba–O/Al_2O_3	63
Ce–Zr–Y–O/Al_2O_3	116	Pd/Ce–Zr–Y–O/Al_2O_3	60
Ce–Zr–La–O/Al_2O_3	111	Pd/Ce–Zr–La–O/Al_2O_3	58
Ce–Zr–Pr–O/Al_2O_3	115	Pd/Ce–Zr–Pr–O/Al_2O_3	54
Ce–Zr–Nd–O/Al_2O_3	118	Pd/Ce–Zr–Nd–O/Al_2O_3	55
Ce–Zr–Sm–O/Al_2O_3	116	Pd/Ce–Zr–Sm–O/Al_2O_3	56

Table 8. Effect of catalyst composition on catalyst reduction under H_2 TPR conditions [112, 113]

Catalyst calcined at 773 K	α peak		β peak		γ peak	
	H_2 uptake, mmol/g	T_α, K	H_2 uptake, mmol/g	T_β, K	H_2 uptake, mmol/g	T_γ, K
Pd/Al_2O_3	46.1	284	–	–	–	–
Pd/Ce–Zr–O/Al_2O_3	24.5	308	13.5	318	8.5	375
Pd/Ce–Zr–Mg–O/Al_2O_3	17.1	291	13.8	317	14.9	370
Pd/Ce–Zr–Ca–O/Al_2O_3	38.5	290	–	–	14.6	374
Pd/Ce–Zr–Sr–O/Al_2O_3	17.5	291	14.9	321	15.0	374
Pd/Ce–Zr–Ba–O/Al_2O_3	17.9	291	15.3	313	14.8	373
Pd/Ce–Zr–Y–O/Al_2O_3	12.2	291	21.8	321	13.8	376
Pd/Ce–Zr–La–O/Al_2O_3	37.6	312	–	–	7.3	378
Pd/Ce–Zr–Pr–O/Al_2O_3	28.5	308	3.6	316	14.8	371
Pd/Ce–Zr–Nd–O/Al_2O_3	3.5	288	28.8	316	12.5	371
Pd/Ce–Zr–Sm–O/Al_2O_3	5.2	291	28.2	318	12.5	372

was prepared by the impregnation of pseudoboehmite with a mixed solution of Ce, Zr, and M nitrates in a specified ratio. As can be seen in Table 7, the introduction of Ce–Zr–O or Ce–Zr–M–O components into Al_2O_3 facilitated an increase in the S_{BET} of not only the support but also the catalyst. In this case, the specific surface area only slightly depended on the nature of M.

According to XRD data, these catalysts did not contain Pd or PdO phases; this was likely due to the low palladium content of the catalysts. The supports calcined at 1173 K were a combination of cubic and tetragonal solid solutions and γ-Al_2O_3. An increase in the treatment temperature to 1373 K only increased the degree of crystallinity of the solid solutions and led to the formation of δ-Al_2O_3. Thus, the introduction of Ce–Zr–O or Ce–Zr–M–O compositions into aluminum oxide stabilized the low-temperature alumina species and prevented the formation of α-Al_2O_3 and $CeAlO_3$.

Yue et al. [112, 113] performed electron-microscopic studies and found that the average particle sizes of Pd in the Pd/Ce–Zr–Ca–O/Al_2O_3 and Pd/Ce–Zr–O/Al_2O_3 samples calcined at 773 K were 8 and 10 nm, respectively. After treatment at 1373 K, these sizes increased to 14 and 25 nm, respectively. Consequently, the additive of Ca inhibited the agglomeration of Pd particles. With the use of H_2 TPR, it was found (Table 8) that Pd/Al_2O_3 was readily reduced at 284 K.

Table 9. Effect of catalyst composition and treatment temperature on catalytic activity in the reaction of methane oxidation [112, 113]

Catalyst calcined at 773 K	T_{50}, K	Catalyst calcined at 1373 K	T_{50}, K
Pd/Al_2O_3	629	$Pd/Ce–Zr–Y–O/Al_2O_3$	641
$Pd/Ce–Zr–Ca–O/Al_2O_3$	633	$Pd/Ce–Zr–Sm–O/Al_2O_3$	651
$Pd/Ce–Zr–Y–O/Al_2O_3$	633	$Pd/Ce–Zr–Ca–O/Al_2O_3$	663
$Pd/Ce–Zr–Ba–O/Al_2O_3$	641	$Pd/Ce–Zr–Nd–O/Al_2O_3$	663
$Pd/Ce–Zr–Mg–O/Al_2O_3$	647	$Pd/Ce–Zr–Pr–O/Al_2O_3$	668
$Pd/Ce–Zr–Sr–O/Al_2O_3$	647	$Pd/Ce–Zr–Mg–O/Al_2O_3$	678
$Pd/Ce–Zr–Sm–O/Al_2O_3$	647	$Pd/Ce–Zr–Sr–O/Al_2O_3$	678
$Pd/Ce–Zr–Nd–O/Al_2O_3$	651	$Pd/Ce–Zr–O/Al_2O_3$	683
$Pd/Ce–Zr–O/Al_2O_3$	663	$Pd/Ce–Zr–Ba–O/Al_2O_3$	683
$Pd/Ce–Zr–Pr–O/Al_2O_3$	663	$Pd/Ce–Zr–La–O/Al_2O_3$	683
$Pd/Ce–Zr–La–O/Al_2O_3$	668	Pd/Al_2O_3	723

The H_2 TPR curves of the $Pd/Ce–Zr–M–O/Al_2O_3$ samples exhibited three peaks in the temperature ranges of 288–312, 316–321, and 370–378 K (α, β, and γ peaks, respectively). Yue et al. [112, 113] assumed that the α peak corresponds to the reduction of PdO supported on the Al-containing component, the β peak corresponds to the reduction of PdO on the Ce–Zr component, and the γ peak corresponds to the reduction of Pd stabilized by zirconium dioxide. An analysis of data given in Table 8 indicated that, upon the introduction of Ce–Zr–O or Ce–Zr–M–O compositions (M = La or Pr) into Al_2O_3, the temperature at which the α peak appeared (T_α) increased, whereas the introduction of Ce–Zr–M–O, where M = Mg, Ca, Sr, Ba, Y, Nd, or Sm, decreased this temperature to 288–391 K. Thus, in the majority of cases, the presence of M in a Ce–Zr composition facilitated the reduction of PdO distributed over the Al-containing component.

The activity of the catalysts in the reaction of methane oxidation depended on the nature of the introduced components and on the treatment temperature (Table 9) [112, 113]. The temperature at which 50% CH_4 conversion was reached varied from 629 to 668 K depending on the nature of the catalyst calcined at 773 K. The most active catalyst was Pd/Al_2O_3. Upon the introduction of Ce–Zr–Ca(Y)–O additives into Al_2O_3, the activity of the catalyst became comparable to the activity of Pd/Al_2O_3; Ce–Zr–Pr(La)–O additives were less effective. A comparison of the activity of these samples with their reducing properties suggests a correlation between T_{50} and T_α: the lower T_α, the higher the activity and vice versa. In turn, a decrease in T_α can be due to an increase in the degree of dispersion of PdO, which depends on the nature of the introduced additive. An increase in the catalyst calcination temperature to 1373 K changed the catalyst activity order: the $Pd/Ce–Zr–Y–O/Al_2O_3$ catalyst became the most active, whereas Pd/Al_2O_3 became less active. Thus, the introduction of a Ce–Zr–Y–O additive into aluminum oxide allows one to obtain an active and stable Pd-containing catalyst for CH_4 oxidation.

Thus, the results of the above studies allow us to make the following conclusions:

(1) A cubic solid solution with the fluorite structure is formed in the $Ce_{1-x}Zr_xO_2$ system at $x < 0.5$, and the stability of this solid solution depends on preparation procedure and treatment conditions (temperature and atmosphere). The subsequent introduction of transition metals (Mn, Ni, and Co) or rare earth elements (La, Y, Pr, and Nd) in a certain concentration into the Ce–Zr–O binary system facilitates the formation of a single-phase solid solution with the fluorite structure and extends the region of its occurrence. The introduction of platinum group metals (by precipitation or impregnation methods) has no effect on the structure of the solid solution.

(2) The texture characteristics of the Ce–Zr–O system mainly depend on thermal treatment conditions: the S_{BET} of the samples decreases with calcination temperature; in this case, the main decrease occurred in the first hours of treatment. The action of steam at 1273 K results in a dramatic decrease in S_{BET} to 3–5 m^2/g. A decrease in the specific surface area is also observed after reduction cycles. The total pore volume of fresh samples depends on the Ce/Zr ratio and treatment temperature and varies over the range of 0.2–0.3 cm^3/g. Upon the introduction of transition metals or rare earth elements, S_{BET} increases or remains unchanged on the thermal treatment of the samples.

(3) The introduction of the isovalent Zr^{4+} cation increases the amount of lattice defects both on the surface and in the bulk of CeO_2. The presence of defects

facilitates an increase in the mobility of oxygen and its diffusion in the lattice to stimulate the reduction of Ce^{4+} in the $Ce_{1-x}Zr_xO_2$ solid solution. The amount of hydrogen consumed for the reduction of the sample depends on the composition, but it is independent of S_{BET}. The value of OSC for $Ce_{1-x}Zr_xO_2$ samples with $0.2 \le x \le 0.4$ is higher than the OSC of individual cerium dioxide by a factor of about 4. The introduction of M^{n+} into the lattice of $Ce_{1-x}Zr_xO_{2-\delta}$ facilitates a decrease in the reduction temperature of the complex oxide system because of the formation of anion vacancies. In this case, the reoxidation of M^+ or M^0 to M^{n+} facilitates the reduction of Ce^{4+} to Ce^{3+}. The introduction of rare earth elements into the lattice of $Ce_{1-x}Zr_xO_{2-\delta}$ has almost no effect on the reduction temperature of the complex oxide composition, whereas a low-temperature peak due to the reduction $N^{\delta+} \longrightarrow N^0$ appears in the TPR curves upon the introduction of platinum group metals.

(4) The adsorption and catalytic properties of the Ce–Zr–M–O and N/Ce–Zr–O (N is a platinum group metal) systems depend on the presence of anion vacancies and the ease of the transitions $Ce^{4+} \rightleftharpoons Ce^{3+}$ and $N^{\delta+} \longrightarrow N^{0+}$. Charged oxygen species are formed upon the adsorption of molecular oxygen. Surface carbonate structures are formed upon the adsorption of CO on $Ce_{1-x}Zr_xO_2$; a considerable energy is required to destroy these structures because the degradation involves oxygen–oxide bond rupture. At elevated temperatures, the decomposition of surface carbonates with the formation of CO_2 occurs rapidly. Upon the adsorption of CO on $N/Ce_{1-x}Zr_xO_2$, linear monocarbonyl complexes; bridging CO sites; and, probably, the complexes of carbon bound to palladium on the sample surface through the oxygen atom appear. The decomposition of these groups occurs at a lower temperature.

REFERENCES

1. Leonov, A.I., Andreeva, A.B., and Keler, E.K., *Khimiya vysokotemperaturnykh materialov* (Chemistry of High-Temperature Materials), Leningrad: Nauka, 1967, p. 91.
2. Trovarelli, A., de Leitenburg, C., Boaro, M., and Dolcetti, G., *Catal. Today*, 1999, vol. 50, p. 353.
3. Bernal, S., Kaspar, J., and Trovarelli, A., *Catal. Today*, 1999, vol. 50, p. 175.
4. Sohier, M.P., Wrobel, G., Bonnelle, J.P., and Marcq, J.P., *Appl. Catal.*, 1992, vol. 84, p. 169.
5. Eur. Patent 8508210, 1986.
6. Harrison, B., Diwell, A.F., and Hallett, C., *Platinum Met. Rev.*, 1988, vol. 32, no. 2, p. 73.
7. Padeste, C., Cant, N.W., and Trimm, D.L., *Catal. Lett.*, 1993, vol. 18, p. 305.
8. Sanchez, M.G. and Gazquez, J.L., *J. Catal.*, 1987, vol. 104, p. 120.
9. Hermann, J.M., Hoang-Van, C., Dibansa, L., and Harivololona, R.J., *J. Catal.*, 1996, vol. 159, p. 361.
10. De Leitenburg, C., Trovarelli, A., Liorca, J., Cavani, F., and Bini, G., *Appl. Catal., A*, 1996, vol. 139, p. 161.
11. Choudhary, T.V., Banerjee, S., and Choudhary, V.R., *Appl. Catal., A*, 2002, vol. 234, p. 1.
12. Eigenmann, F., Maciejewski, M., and Baiker, A., *Appl. Catal., B*, 2006, vol. 62, p. 311.
13. Diagne, C., Idriss, H., and Kiennemann, A., *Catal. Commun.*, 2002, vol. 3, p. 565.
14. Courcot, D., Abi-Aad, E., Capelle, S., and Aboukais, A., *Stud. Surf. Sci. Catal.*, 1998, vol. 116, p. 625.
15. Trovarelli, A., *Catal. Rev. Sci. Eng.*, 1996, vol. 38, p. 439.
16. Leonov, A.I., *Vysokotemperaturnaya khimiya kislorodnykh soedinenii tseriya* (High-Temperature Chemistry of Cerium–Oxygen Compounds), Leningrad: Nauka, 1970, p. 4.
17. Zachariasen, W., *Z. Phys. Chem.*, 1926, vol. 123, p. 134.
18. Bevan, D.J.M., *J. Inorg. Nucl. Chem.*, 1955, vol. 1, p. 49.
19. *Spravochnik khimika* (Chemist's Handbook), Perel'man, V.I., Ed., Leningrad: Khimiya, 1971, p. 381.
20. *JCPDS File 28–271*, Pennsylvania State Univ., 1975.
21. Voronkov, A.A., Shumyatskaya, N.G., and Pyatenko, Yu.A., *Kristallokhimiya mineralov tsirkoniya i ikh iskusstvennye analogi* (Crystal Chemistry of Zirconium Minerals and Their Artificial Analogues), Moscow: Nauka, 1978, p. 3.
22. Glushkova, V.B. and Sazonova, L.V., in *Khimiya vysokotemperaturnykh materialov* (Chemistry of Macromolecular Materials), Leningrad: Nauka, 1967, p. 83.
23. Fujimori, A., *Phys. Rev.*, 1983, vol. 28, p. 2281.
24. Kotani, A., Mizuta, H., Jo, T., and Parlebas, J.C., *Solid State Commun.*, 1985, vol. 53, p. 805.
25. Wuilloud, E., Delley, B., Schneider, W.D., and Daer, Y., *Phys. Rev. Lett.*, 1984, vol. 53, p. 202.
26. Koelling, D., Boring, A., and Wood, J., *Solid State Commun.,* 1983, vol. 47, p. 227.
27. Hill, S. and Catlow, C.R.A., *J. Phys. Chem. Solids*, 1993, vol. 54, p. 411.
28. Sayle, T., Parker, S., and Catlow, C.R.A., *Surf. Sci.*, 1994, vol. 316, p. 329.
29. Conesa, J., *Surf. Sci.*, 1995, vol. 339, p. 337.
30. Konner, R., Ricken, M., Nolting, J., and Riess, I., *J. Solid State Chem.*, 1989, vol. 78, p. 136.
31. Faber, J., Seitz, M., and Mueller, M., *J. Phys. Chem.*, 1976, vol. 37, p. 909.
32. Hermann, J., Ramaroson, E., Tempere, J., and Guilleux, M., *Appl. Catal.*, 1989, vol. 53, p. 117.
33. Sayle, T., Parker, S., and Catlow, C.R.A., *J. Chem. Soc., Chem. Commun.*, 1992, p. 977.
34. Trovarelli, A., Boaro, M., Rocchini, E., de Leitenburg, C., and Dolcetti, G., *J. Alloys Compd.*, 2001, vols. 323–324, p. 584.
35. Perrichon, V., Laachir, A., Abournadasse, S., Touret, O., and Blanchard, G., *Appl. Catal.*, 1995, vol. 129, p. 69.

36. Terrible, D., Trovarelli, A., Llorca, J., de Leitenburg, C., and Dolcetti, G., *J. Catal.*, 1998, vol. 178, p. 299.
37. Cho, B.K., *J. Catal.*, 1991, vol. 131, p. 74.
38. Nunan, J.G., Williamson, W.B., and Robota, H.J., *SAF Paper no. 960798*, 1998.
39. Duwez, P. and Odell, F., *J. Am. Ceram. Soc.*, 1952, vol. 35, p. 107.
40. Yashima, M., Arashi, H., Kakihana, M., and Yoshimura, M., *J. Am. Ceram. Soc.*, 1994, vol. 77, p. 1067.
41. Tani, E., Yoshimura, M., and Somiya, S., *J. Am. Ceram. Soc.*, 1983, vol. 66, p. 506.
42. Duran, P., Gonzales, M., Moure, C., Jurdo, J.R., and Pascal, C., *J. Mater. Sci.*, 1990, vol. 25, p. 5001.
43. Meriani, S., *J. Phys.*, 1986, vol. 47, p. C1-485.
44. Meriani, S., *Mater. Sci. Eng., A*, 1989, vol. 109, p. 121.
45. Meriani, S., *Mater. Sci. Eng.*, 1985, vol. 71, p. 369.
46. Fornasiero, P., Balducci, G., Di Monte, R., Kaspar, J., Sergo, V., Gubitosa, G., Ferrero, A., and Graziani, M., *J. Catal.*, 1996, vol. 164, p. 173.
47. Vlaic, G., Di Monte, R., Fornasiero, P., Fonda, E., Kaspar, J., and Graziani, M., *J. Catal.*, 1999, vol. 182, p. 378.
48. Turko, G.A., Ivanova, A.S., Plyasova, L.M., Litvak, G.S., and Rogov, V.A., *Kinet. Katal.*, 2005, vol. 46, no. 6, p. 932 [*Kinet. Catal.* (Engl. Transl.), vol. 46, no. 6, p. 884].
49. Bozo, C., Caillard, F., and Guilhaume, N., *Appl. Catal., A*, 2001, vol. 220, p. 69.
50. Zyuzin, D.A., Moroz, E.M., Ivanova, A.S., and Zaikovskii, V.I., *Neorg. Mater.*, 2000, vol. 36, no. 4, p. 447 [*Inorg. Mater.* (Engl. Transl.), vol. 36, no. 4, p. 359].
51. Zyuzin, D.A., Moroz, E.M., Ivanova, A.S., Shmakov, A.N., and Kustova, G.N., *Kinet. Katal.*, 2004, vol. 45, no. 5, p. 780 [*Kinet. Catal.* (Engl. Transl.), vol. 45, no. 5, p. 739].
52. Kol'ko, V.P., Moroz, E.M., Kriventsov, V.V., and Zyuzin, D.A., *Izv. Akad. Nauk, Ser. Fiz.*, 2007, vol. 71, no. 5, p. 718.
53. Fornasiero, P., Di Monte, R., Rao, G.R., Kaspar, J., Meriani, S., Trovarelli, A., and Graziani, M., *J. Catal.*, 1995, vol. 151, p. 168.
54. Hartridge, A. and Bhattacharya, A.K., *J. Phys. Chem. Solids*, 2002, vol. 63, p. 441.
55. Rossignol, S., Madier, Y., and Duprez, D., *Catal. Today*, 1999, vol. 50, p. 261.
56. Fornasiero, P., Balducci, G., Di Monte, R., Kaspar, J., Sergo, V., Gubitosa, G., Ferrero, A., and Graziani, M., *J. Catal.*, 1995, vol. 164, p. 173.
57. Balducci, G., Fornasiero, P., Di Monte, R., Kaspar, J., Meriani, S., and Graziani, M., *Catal. Lett.*, 1995, vol. 33, p. 193.
58. Ivanova, A.S., Moroz, E.M., and Litvak, G.S., *Kinet. Katal.*, 1992, vol. 33, p. 1208.
59. Mirota, T., Hasegawa, T., Aozasa, S., Matsui, H., and Motoyama, M., *J. Alloys Compd.*, 1993, vol. 193, p. 298.
60. Yashima, M., Morimoto, K., Nobuo, N., and Yoshimura, M., *J. Am. Ceram. Soc.*, 1993, vol. 76, no. 7, p. 1745.
61. Yashima, M., Morimoto, K., Ishizawa, N., and Yoshimura, M., *J. Am. Ceram. Soc.*, 1993, vol. 76, no. 11, p. 2865.
62. Vidal, H., Kaspar, J., Pijolat, M., Colon, G., Bernal, S., Cordon, A., Perrichon, V., and Fally, F., *Appl. Catal., B*, 2000, vol. 27, p. 49.
63. Terrible, D., Trovarelli, A., Llorca, J., de Leitenburg, C., and Dolcetti, G., *Catal. Today*, 1998, vol. 43, p. 79.
64. Colon, G., Valdivieso, F., Pijolat, M., Baker, R.T., Calvino, J.J., and Bernal, S., *Catal. Today*, 1999, vol. 50, p. 271.
65. Di Monte, R. and Kaspar, J., *Catal. Today*, 2005, vol. 100, p. 27.
66. Kaspar, J., Fornasiero, P., and Graziani, M., *Catal. Today*, 1999, vol. 50, p. 285.
67. Jen, H.-W., Graham, G.W., Chun, W., McCabe, R.W., Cuif, J.-P., Deutsch, S.E., and Touret, O., *Catal. Today*, 1999, vol. 50, p. 309.
68. Ozawa, M. and Loong, C.-K., *Catal. Today*, 1999, vol. 50, p. 329.
69. Yao, H.C. and Yu, YaoY.F., *J. Catal.*, 1984, vol. 86, p. 254.
70. Trovarelli, A., *Catal. Rev. Sci. Eng.*, 1996, vol. 38, p. 439.
71. Rao, G.R., Kaspar, J., Meriani, S., Di Monte, R., and Graziani, M., *Catal. Lett.*, 1994, vol. 24, p. 107.
72. De Leitenburg, C., Goi, D., Primavera, A., Trovarelli, A., and Dolcetti, G., *Appl. Catal., B*, 1996, vol. 11, p. L29.
73. Boaro, M., de Leitenburg, C., Dolcetti, G., and Trovarelli, A., *J. Catal.*, 2000, vol. 193, p. 338.
74. Madier, Y., Descorme, C., Le Govic, A.M., and Duprez, D., *J. Phys. Chem. B*, 1999, vol. 103, p. 10999.
75. Descorme, C., Madier, Y., and Duprez, D., *J. Catal.*, 2000, vol. 196, p. 167.
76. Li, C., Domen, K., Maruya, K.-I., and Onishi, T., *J. Am. Chem. Soc.*, 1989, vol. 111, p. 7683.
77. Li, C., Domen, K., Maruya, K.-I., and Onishi, T., *J. Catal.*, 1990, vol. 123, p. 436.
78. Imamura, S., Shono, M., Okamoto, N., Haneda, A., and Ishida, S., *Appl. Catal., A*, 1996, vol. 142, p. 279.
79. Machida, M., Uto, M., Kurogi, D., and Kijima, T., *Chem. Mater.*, 2000, vol. 12, p. 3158.
80. Qi, G. and Yang, R.T., *J. Catal.*, 2003, vol. 217, p. 434.
81. Qi, G., Yang, R.T., and Chang, R., *Appl. Catal., B*, 2004, vol. 51, p. 93.
82. Qi, G. and Yang, R.T., *J. Phys. Chem. B*, 2004, vol. 108, no. 40, p. 15738.
83. Lamonier, C., Ponchel, A., Huysser, A., and Jalowiecki-Duhamel, L., *Catal. Today*, 1999, vol. 50, p. 247.
84. Lamonier, C., Bennani, A., Huysser, A., Aboukais, A., and Wrobel, G., *J. Chem. Soc., Faraday Trans.*, 1996, vol. 92, p. 131.
85. Kacimi, S., Duprez, D., and Dalmon, J.A., *J. Chem. Phys.*, 1997, vol. 94, p. 535.
86. Takeguchi, T., Furukama, S., and Inoue, M., *J. Catal.*, 2001, vol. 202, p. 14.
87. Sermon, P.Q. and Bond, G.C., *Catal. Rev. Sci. Eng.*, 1973, vol. 8, p. 211.
88. Bianchi, D., Gardes, G.E., Pajonk, G.M., and Teichner, S.J., *J. Catal.*, 1975, vol. 38, p. 135.

89. Kulyova, S.P., Lunina, E.V., Lunin, V.V., Kostyuk, B.G., Muravyova, G.P., Kharlanov, A.N., Zhilinskaya, E.A., and Aboukais, A., *Chem. Mater.*, 2001, vol. 13, p. 1491.

90. Ikryannikova, L.M., Aksenov, A.A., Markaryan, G.L., Kostyuk, B.G., Kharlanov, A.N., and Lunina, E.V., *Appl. Catal., A*, 2001, vol. 210, p. 225.

91. Rohart, E., Larcher, O., Deutsch, S., Hedouin, C., Aimin, H., Fajardie, F., Allain, M., and Macaudiere, P., *Top. Catal.*, 2004, vols. 30/31, p. 417.

92. Ivanova, A.S., *Kinet. Katal.*, 2001, vol. 42, no. 3, p. 394 [*Kinet. Catal.* (Engl. Transl.), vol. 42, no. 3, p. 354].

93. Turko, G.A., Ivanova, A.S., Plyasova, L.M., Litvak, G.S., Rogov, V.A., Slavinskaya, E.M., Polukhina, I.A., and Noskov, A.S., *Kinet. Katal.*, 2007, vol. 48, no. 1, p. 150 [*Kinet. Catal.* (Engl. Transl.), vol. 48, no. 1, p. 143].

94. Primavera, A., Trovarelli, A., de Leitenburg, C., Dolcetti, G., and Llorca, J., *Stud. Surf. Sci. Catal.*, 1998, vol. 119, p. 87.

95. Bozo, C., Guilhaume, N., and Herrmann, J.-M., *J. Catal.*, 2001, vol. 203, p. 393.

96. Noronha, F.B., Fendley, E.C., Soares, R.R., Alvarez, W.E., and Resasco, D.E., *Chem. Eng. J.*, 2001, vol. 82, p. 21.

97. Diagne, C., Idriss, H., and Kiennemann, A., *Catal. Commun.*, 2002, vol. 3, p. 565.

98. Rao, G.R., Fornasiero, P., Monte, R.D., Kaspar, J., Vlaic, G., Balducci, G., Meriani, S., Gubitosa, G., Cremona, A., and Graziani, M., *J. Catal.*, 1996, vol. 162, p. 1.

99. Nunan, J.G., Robota, H.J., Cohn, M.J., and Bradley, S.A., *J. Catal.*, 1992, vol. 133, p. 309.

100. Bernal, S., Calvino, J.J., Cifredo, G.A., Rodriguez-Izqueirdo, J.M., Perrichon, V., and Laachir, A., *J. Catal.*, 1992, vol. 137, p. 1.

101. Ho, C., Yu, J.C., Wang, X., Lai, S., and Qiu, Y., *J. Mater. Chem.*, 2005, vol. 15, p. 2193.

102. Liu, Y., Hayakawa, T., Ishii, T., Kumagai, M., Yasuda, H., Suzuki, K., Hamakawa, S., and Murata, K., *Appl. Catal., A*, 2001, vol. 210, p. 301.

103. Imamura, S., Higashihara, T., Saito, Y., Aritani, H., Kanai, H., Matsumura, Y., and Tsuda, N., *Catal. Today*, 1999, vol. 50, p. 369.

104. Fornasiero, P., Kaspar, J., Sergo, V., and Graziani, M., *J. Catal.*, 1999, vol. 182, p. 56.

105. Hickey, N., Fornasiero, P., Kaspar, J., Gatica, J.M., and Bernal, S., *J. Catal.*, 2001, vol. 200, p. 181.

106. Lieske, H., Lietz, G., Spindler, H., and Voelter, J., *J. Catal.*, 1983, vol. 182, p. 8.

107. Busca, G. and Lorenzelli, V., *J. Mater. Chem.*, 1982, vol. 7, p. 89.

108. Karpinski, Z., *Adv. Catal.*, 1990, vol. 37, p. 45.

109. Kiennemann, A., Breault, R., and Hindermann, J.P., *J. Chem. Soc., Faraday Trans.*, 1987, vol. 83, p. 2119.

110. Bernal, S., Blanco, G., Calvino, J.J., Gatica, J.M., Omil, J.A., and Pintado, J.M., *Top. Catal.*, 2004, vol. 28, p. 31.

111. Xiao, L., Sun, K., Yang, Y., and Xu, X., *Catal. Lett.*, 2004, vol. 95, p. 151.

112. Yue, B., Zhou, R., Wang, Y., and Zheng, X., *J. Mol. Catal. A: Chem.*, 2005, vol. 238, p. 241.

113. Yue, B., Zhou, Ra., Wang, Y., and Zheng, X., *Appl. Catal., A*, 2005, vol. 295, p. 31.